

## Article

# High-Beam-Quality and High-Brightness 532 nm Laser with Output Power 96 W

Hongcai Liu <sup>1,2,3</sup>, Qingxuan Li <sup>1,2,3,4</sup>, Yu Ding <sup>5</sup>, Xuesheng Liu <sup>1,2,3,\*</sup>, Jiapeng Hu <sup>1,2,3</sup>, Boyi Yang <sup>1,2,3</sup>, Youqiang Liu <sup>1,2,3</sup> and Zhiyong Wang <sup>1,2,3</sup>

<sup>1</sup> Beijing Engineering Research Center of Laser Technology, Beijing University of Technology, Beijing 100124, China

<sup>2</sup> Key Laboratory of Trans-Scale Laser Manufacturing Technology, Beijing University of Technology, Ministry of Education, Beijing 100124, China

<sup>3</sup> Institute of Advanced Technology on Semiconductor Optics & Electronics, Institute of Laser Engineering, Beijing University of Technology, Beijing 100124, China

<sup>4</sup> The 53rd Research Institute of China Electronics Technology Group Corporation, Tianjin 300308, China

<sup>5</sup> Science and Technology on Electro-Optical Information Security Control Laboratory, Tianjin 300308, China

\* Correspondence: 13810435431@163.com; Tel.: +86-13810435431

**Abstract:** We developed a high-power, double-intracavity-frequency, diode-side-pumped, Q-switched Nd:YAG laser. The thermal birefringence effect of Nd:YAG crystal was compensated by a quartz rotating mirror, and the stable cavity structure was designed according to the thermal focal length of a single module. A 532 nm laser with a maximum linearly polarized output power of 96 W was obtained at a pumping power of 1300 W and repetition rate of 10 kHz. The pulse width was 55.8 ns, and the beam quality was measured to be  $M^2_x = 5.98$ ,  $M^2_y = 8.14$  at the maximum output power; therefore, a brightness as high as  $6.97 \times 10^8 \text{ W}\cdot\text{cm}^{-2}\cdot\text{Sr}$  was achieved. To the best of our knowledge, this is the highest brightness obtained for a high-power Nd:YAG laser at 532 nm.

**Keywords:** Nd:YAG laser; diode-side-pumped; intracavity frequency conversion; high brightness



**Citation:** Liu, H.; Li, Q.; Ding, Y.; Liu, X.; Hu, J.; Yang, B.; Liu, Y.; Wang, Z. High-Beam-Quality and High-Brightness 532 nm Laser with Output Power 96 W. *Crystals* **2023**, *13*, 290. <https://doi.org/10.3390/cryst13020290>

Academic Editors: Ludmila Isaenko and Shin-Tson Wu

Received: 29 December 2022

Revised: 4 February 2023

Accepted: 7 February 2023

Published: 8 February 2023



**Copyright:** © 2023 by the authors. Licensee MDPI, Basel, Switzerland. This article is an open access article distributed under the terms and conditions of the Creative Commons Attribution (CC BY) license (<https://creativecommons.org/licenses/by/4.0/>).

## 1. Introduction

A high-power green laser with a high repetition rate, short pulse duration, and reasonably good beam quality is important for various industrial and scientific applications. High-power green lasers have been widely used in many fields, such as material processing [1], laser medicine [2,3], and military defense [4]. In addition, they can also be used as a pump source to realize the laser output in ultraviolet and deep ultraviolet bands [5].

Nd:YAG is the most commonly used active material for high-power green lasers due to its good optical and thermal properties and low price [6,7]. Although many different pumping schemes and laser types are available at present, the diode-side-pumped Nd:YAG rod laser is a very competitive technology due to its reliability, high power, and simplicity, and the low cost of its components [8–10]. The intracavity frequency doubling of a diode-pumped, repetitively Q-switched Nd:YAG laser operating at 1064 nm is an efficient way to generate a green beam with high average power, high efficiency, and good stability.  $\text{KTiOPO}_4$  (KTP) crystal and  $\text{LiB}_3\text{O}_5$  (LBO) crystal are often chosen as second-harmonic-generation nonlinear crystals. The former has a high effective nonlinear coefficient, large acceptance angle and high temperature bandwidth [11]. The frequency conversion efficiency of KTP crystal is higher than that of LBO crystal. However, the graytracking problem, which leads to a photochromic effect at a threshold intensity of  $80 \text{ MW}/\text{cm}^2$ , limits the lifetime of the KTP crystal for high-average-power second harmonic generation [12]. LBO is one of the most promising candidates, especially for high-average-power second harmonic generation, owing to its high damage threshold (greater than  $2.5 \text{ GW}/\text{cm}^2$ ). Considering the advantages and disadvantages of KTP crystal and LBO crystal, LBO crystal was finally used in this experiment to obtain a high average power and long lifetime for a 532 nm laser.

Furthermore, to qualify for industrial applications, these diode-pumped solid-state green lasers should have a high output power and compact size, be immune to environmental fluctuations, and have low pulse-to-pulse timing and amplitude jitter, as well as a high beam-pointing stability and low output-power drift during their long-term operation, in addition to a simple design that can easily be reproduced using off-the-shelf components.

In recent years, domestic and foreign researchers have conducted research on a solid-state green laser and made a lot of progress. In 2005, Zhenyu Y et al. [13] designed a resonant cavity structure with high collimation stability, according to the change in the thermal lens focal length of the laser working substance with the pumping power of the pump source. Using this resonant cavity structure and adding an acousto-optic Q-switch, they successfully achieved a Q-switched green laser output with a power of 162 W at a repetition rate of 10 kHz, with a pulse width of 80 ns and beam quality of  $M^2 = 20$ . In 2006, Geng A et al. [14] designed a dual-V-shaped configuration to ensure a high average power and long-lifetime second harmonic generation. In a thermally near-unstable resonator, a large fundamental mode size in the Nd:YAG rod and a small size of LBO crystal could be used, which improved both the beam quality and the power density. This structure was used to obtain a 121 W green laser output with  $M^2 = 20$  and a pulse width of 68 ns at the repetition rate of 10 kHz. In 2007, Yong B et al. [15] developed a high-power and high-efficiency laser head using a numerical simulation of the gain distribution of the diode-side-pumped Nd:YAG rod. They designed a thermal, near-unstable resonator with double-rod birefringence compensation, and then obtained a green laser output with an average power of 218 W with  $M^2 = 20$  using the intracavity frequency-doubling technique. In 2008, Zhongyao Feng et al. [16] demonstrated a laser diode, side-pumped, two-rod, quasi-continuous-wave Nd:YAG green laser. The green laser output power of 164 W was measured at a single laser diode pumping current of 21.6 A, with a repetition rate of 27.2 kHz, pulse width of 130 ns, optical-to-optical conversion efficiency of 13.7 %, beam quality factors of  $M^2_x = 9.52$  and  $M^2_y = 9.86$ , and output power fluctuation of 2.3%. In 2014, Sharma K et al. [17] designed an acousto-optic Q-switched Nd:YAG laser, combined with an LBO crystal, to obtain a 160 W green laser output with repetition rates of 20 kHz, pulse duration of 73 ns, and beam quality of 18. The optical-to-optical conversion efficiency was 12.7%. In 2017, Yuan X et al. [18] demonstrated a high-power laser at 532 nm by frequency doubling an acousto-optic Q-switched and side-pumped Nd:YAG laser at 1064 nm, using a compact linear cavity. The average output power of the pulsed fundamental laser at 1064 nm was as high as 299 W. The laser employed two acousto-optic Q-switches, placed orthogonally to each other to improve their hold-off capacity. Using intracavity frequency doubling with a type II non-critically phase-matched LBO crystal, 165 W average power was generated for the frequency-doubled output at 532 nm, with a repetition rate of 20 kHz and pulse width of 160 ns, which corresponds to a pulse energy of 8.25 mJ and peak power of 51.6 kW, respectively. In 2019, Singh A et al. [19] developed an intracavity frequency-doubled acousto-optic Q-switched Nd:YAG laser, generating 260 W of average green power using two identical diode-pumped gain modules with fivefold pumping symmetry in a simple two-mirror linear cavity configuration. At maximum output power, individual green-pulse duration was measured to be 73 ns, with a pulse repetition rate of 18 kHz and beam quality of  $M^2 = 35$ . The laser was highly stable, with measured fluctuations in average green power  $\pm 0.83$  W over 5 h of continuous operation. The jitter in pulse delay time and pulse-to-pulse amplitude fluctuations were measured to be within  $\pm 4.25$  ns and  $\pm 5\%$ , respectively.

In previous studies, the beam quality of the 532 nm high-power laser was poor. In this paper, a reasonable resonator was designed, considering the thermal effect of the crystal to obtain a 532 nm laser with high power and high beam quality. Furthermore, the laser had the highest brightness obtained to date, to the best of our knowledge.

In this paper, to obtain a high-power and high-beam-quality green laser, a reasonable resonator was designed, considering the thermal effect of the crystal. An average power of 96 W was obtained at 532 nm, with a pulse width of 55.8 ns and a repetition rate of 10 kHz.

At the maximal power, beam quality factors  $M_x^2 = 5.98$ ,  $M_y^2 = 8.14$  were measured, and a brightness as high as  $6.97 \times 10^8 \text{ W}\cdot\text{cm}^{-2}\cdot\text{Sr}$  was achieved.

## 2. Theoretical Analysis

At present, how to increase the output power and improve the beam quality of an all-solid-state green laser is the research focus. To achieve high output power in a solid-state green laser, it is necessary to increase the pumping power and the number of pumping diodes. In this case, the diode-side-pumped Nd:YAG laser was shown to be effective. A high-power laser output can be obtained using two rods. However, due to the non-uniform absorption of the laser working substance by the pump light, only part of the energy input that was pumped into the crystal was converted into laser oscillation, and the rest of the energy was converted into heat loss, which leads to an uneven temperature distribution in the laser crystal. This phenomenon is called the thermal effect, which includes three main aspects: thermal lensing, thermal deformation, and thermal birefringence. The influence of thermal deformation is relatively low, and can be ignored when considering the influence of thermal effect on cavity [20]. In particular, the pump-power-induced thermal lensing effect greatly influences the laser performance; as a result of this, the laser mode size at various locations inside the resonator varies dynamically with the pump power, and the cavity becomes unstable as the pump power approaches a critical value. Therefore, when the laser operates at high power, the thermal effect of the laser crystal is one of the main factors to be considered in the design and optimization of the laser system.

For solid-state lasers, the structure of the resonator is changed by the thermal effect caused by optical pumping; therefore, it is necessary to study the dynamic working characteristics of the resonator using the thermal stabilizer mirror and the parameters of the output beam. The reasonable selection of the resonator's structural parameters is important in solid-state laser technology.

Thermal lensing is an optical effect caused by the inhomogeneity of temperature and stress in the laser rods. The laser medium is equivalent to a thermal lens, whose thermal focal length can be calculated using the following formula:

$$f = \frac{KA}{P_a} \left[ \frac{1}{2} \frac{dn}{dT} + n^3 \alpha_T C_{r,\phi} + \frac{\alpha_T r(n-1)}{L} \right]^{-1} \quad (1)$$

where  $K$  represents the thermal conductivity of the laser working substance,  $A$  represents the cross-section area of the laser working substance,  $P_a$  represents the total heat dissipated by the laser working substance,  $dn/dT$  represents the gradient value of the refractive index with temperature,  $\alpha_T$  is the thermal expansion coefficient of the laser working substance, and  $C_{r,\phi}$  is the photoelastic coefficient related to the radius and tangential direction.

To obtain high-power and high-beam-quality green light output, the resonator was designed and optimized according to the thermal effect of laser crystal. In this experiment, a quartz rotating mirror was added between two crystal rods to compensate for their thermal birefringence. The pumped region of the Nd:YAG rod can be considered a thick lens with a transfer matrix [21], given by

$$[M_L]_{r,\phi} = \begin{bmatrix} 1 - \frac{h}{f_{r,\phi}} & \frac{L}{n} \\ -\frac{1}{f_{r,\phi}} & 1 - \frac{h}{f_{r,\phi}} \end{bmatrix} \quad (2)$$

where  $h = L/2n$ , which is the distance between the main plane of the lens and the end face of the crystal rod.  $L$  is the length of the Nd:YAG rod, and  $n$  is the refractive index of the Nd:YAG rod.  $f_{r,\phi}$  is the focal length of the thermal lens for tangential and azimuthal polarization, respectively. For azimuthal polarization, the thermal focal length  $f_\phi$  can be calculated from the relation  $f_\phi/f_r = 1.2$  [22]. In a pumped Nd:YAG rod for the tangential polarization, the variations in measured thermal focal power, as a diode power function for non-lasing conditions, are shown in Figure 1. The thermal focal power linearly increases with the pumping current.

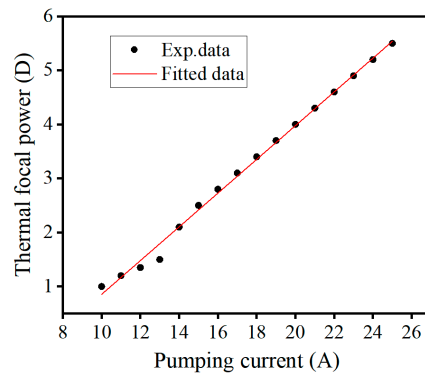


Figure 1. Variation in thermal focal power with pumping current.

In the high-power green laser, the thermal-lensing effect of the frequency-doubling crystal cannot be ignored, but the influence of the thermal effect can be reduced by controlling the temperature and tilt angle of the frequency-doubling crystal. The thermal effect is ignored in the work. The thermal lens equivalent diagram of the resonator is shown in Figure 2.

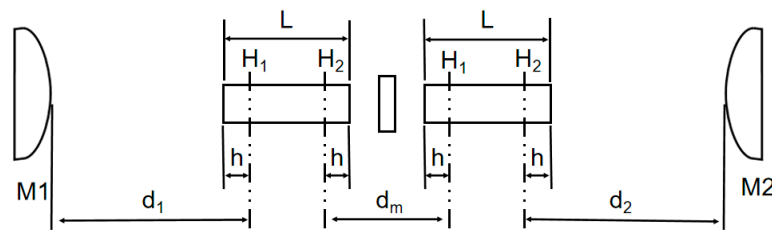


Figure 2. Thermal lens equivalent diagram of resonator.

When the center of the left laser rod is used as the reference plane, the round-trip propagation matrix is given by:

$$\begin{bmatrix} A & B \\ C & D \end{bmatrix} = [M_L]_r d_m [M_L]_\phi d_2 M_R d_2 [M_L]_\phi d_m [M_L]_r d_1 M_R d_1 \tag{3}$$

where  $M_R = \begin{bmatrix} 1 & 0 \\ -\frac{2}{R} & 1 \end{bmatrix}$ ,  $d_i = \begin{bmatrix} 1 & d_i \\ 0 & 1 \end{bmatrix}$  ( $i = 1, 2, m$ ), and  $R$  is the curvature radius of mirror 1 and mirror 2. Matrices represent the transfer matrices for mirrors M1 and M2. The matrices  $[d_1]$  and  $[d_2]$  represent the ray propagation matrices for the free space between mirror M1, the main plane of pump head 1 and pump head 2, and mirror M2, respectively. Matrix  $[d_m]$  represents the ray propagation matrices between the two main planes of the pump heads.

The laser resonator was designed by incorporating measured variations in thermal focal length, along with the pump power required to operate at a high pumping current, using the following resonator stability criteria:

$$-1 < \frac{A + D}{2} < 1 \tag{4}$$

This is the stability condition of the laser resonator. The light will go back and forth several times in the two mirror cavities, satisfying this condition; therefore, the geometric loss of the stable cavity is smaller. The relationship between the q parameters of the TEM<sub>00</sub> Gaussian mode and every element of the round trip matrix is:

$$\frac{1}{q} = \frac{D - A}{2B} \pm i \frac{\sqrt{4 - (A + D)^2}}{2B} \tag{5}$$

Therefore, the beam waist of the Gaussian mode in the laser rod is:

$$\omega = \sqrt{\frac{\lambda}{\pi} \frac{2B}{\sqrt{(4 - (A + D))^2}}} \quad (6)$$

The laser spot size anywhere in the resonator can be obtained by changing the inception reference place of the round-trip matrix. The laser beam distribution can be calculated at any position within the cavity.

According to the transmission matrix and geometric parameters of the resonant cavity, the stability region diagram can be obtained, as shown in Figure 3a. The variation of spot size along the length of cavity at the maximum pumping current is also simulated, as shown in Figure 3b. Through the simulation results, the position of each device in the resonator can be obtained. Figure 3c shows the variation in the TEM<sub>00</sub> mode radius at the left end of the Nd:YAG rod for LH1.

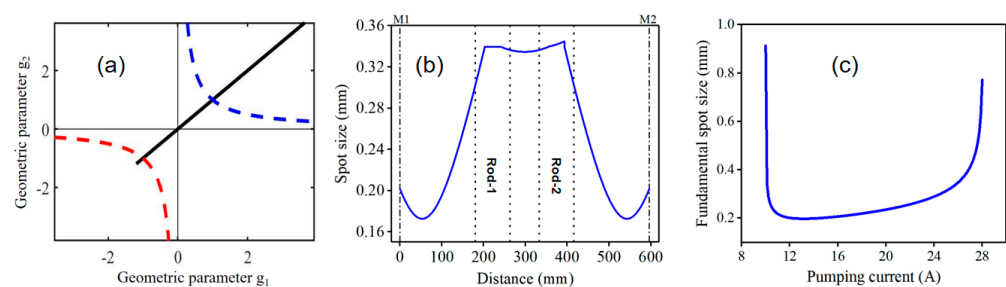


**Figure 3.** (a) Stability region diagram of resonator. (b) Variation of spot size along the length of cavity at the maximum pumping current. (c) Variation in fundamental mode size with pumping current.

The laser was designed in a convex-convex linear cavity configuration, aiming to obtain a tight spot size at the nonlinear crystal to obtain a higher laser power at 532 nm. At the same time, a better beam quality can be obtained using this type of cavity. To obtain a high-power and high-stability laser, combined with simulation and experiment, the length of the total cavity was finally determined to be 596 mm (the distance between the two Nd:YAG rods is 70 mm, the distance from M1 to the left-end face of the LH1 was 180 mm, and the distance from the right-end face of the LH2 to M2 was 180 mm). According to Figure 3b, the LBO crystal is placed at the smallest spot size, about 55 mm from the lens M2.

### 3. Experimental Setup

The experimental apparatus of a double-intracavity-frequency, diode-side-pumped, Q-switched Nd:YAG laser is shown in Figure 4. LH1 and LH2 (RBA35-1C2) are two high-power-laser side-pumping modules. The laser crystals are rod-shaped Nd:YAG crystals with a size of  $\Phi 3 \times 83$  mm and a doping concentration of Nd<sup>3+</sup> of 0.8%. The front and back faces were coated with 1064 nm anti-reflection film to reduce the reflection loss at both ends of the crystal. The laser rod was placed at the center of a flow tube, which can reduce the thermal lensing effect of the laser crystal. A quartz rotator was inserted between the two modules to compensate for the thermal birefringence effect, allowing for the output power and beam quality to be improved. The quartz polarization rotator rotated the two components of the laser electric field by 90°. This could cancel out the phase difference produced by the two laser rods, to compensate for the thermal effect.

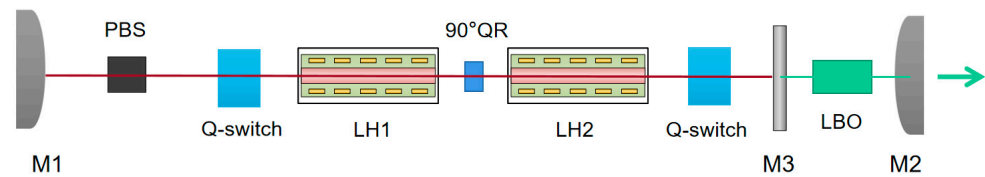


**Figure 4.** Schematic of the laser setup.

In the experiment, two acousto-optic Q switches were used to obtain the peak power laser. The driving frequency was 27.4 MHz, the maximum driving radio frequency (RF) power was 100 W, and a modulation pulse width of  $\leq 100$  ns could be achieved. The acousto-optic modulation frequency of this experiment was set at 10 kHz. The two acousto-optic switches were placed vertically, and the diffraction efficiency of 1064 nm laser was improved by double acousto-optic vertical diffraction. The acousto-optic Q switches were placed close to the crystal rods to improve the diffraction efficiency. To effectively cool the acousto-optic Q switch, its cooling channel had a stainless steel coating, which completely solved the problem of channel corrosion.

M1 is a mirror with high reflectivity at 1064 nm. Mirror M2 is the output mirror, with the surface coated for high reflectance at 1064 nm and high transmittance at 532 nm. The curvature radius of both mirror M1 and mirror M2 was 280 mm. M3 is a flat mirror coated for high transmittance at 1064 nm and high reflectivity at 532 nm. The nonlinear frequency-doubling crystal was an LBO crystal cut for type-I phase-matching with the size of 4 mm  $\times$  4 mm  $\times$  18 mm. To increase the cooling capacity of the LBO crystal, each side of LBO was wrapped with a layer of indium foil stuck in a copper heat sink, and the temperature was accurately controlled by the thermo-electric cooler (TEC). In this experiment, the temperature set by the LBO was 39.8 °C. During the experiment, the angle of the LBO crystal was finely adjusted to meet the phase matching, to improve the frequency conversion efficiency as much as possible. Finally, the purpose of the polarization beam-splitter (PBS) was to provide a linearly polarized 1064 nm laser to the LBO crystal.

#### 4. Results and Discussion

In the experiment, the curve of 1064 nm and 532 nm laser output power versus the total pumping power of two rods was depicted, which is demonstrated in Figure 5. The 1064 nm laser showed tangential polarization in the LH1 and azimuthal polarization in the LH2, and the final output of the 532 nm laser was tangential polarization. The threshold electrical pump power of the 1064 nm laser was 600 W, and that of the 532 nm laser was 750 W. The reason for this phenomenon is that the threshold power of the laser becomes higher after the LBO crystal is added. The output power increases, nearly in proportion to the pumping power. When the electrical pump power is 1300 W, the output power of the 1064 nm laser is 157 W, and the maximum output power of the 532 nm laser can reach 96 W; therefore, the frequency-doubling efficiency is 61%. The optical elements in the laser are controlled by the constant water-cooling temperature, and the optical elements are fixed by a reliable stainless steel adjusting frame. Therefore, the laser power can be reproduced, and the maximum fluctuation range of the laser power is within 0.5 W. However, it can be seen that the power of the 532 nm laser decreases when the electrical pump power is near 1200 W. The characteristic of the laser-unstable cavity is that the output power will further increase with the increase in current after the laser operating point crosses the unstable region. When the electric pump power is 1200 W, the output power is 83 W; then, it enters the unstable zone and the output power decreases. When the electric pump power is 1250 W, the power decreases to the lowest, 70 W, and then enters the stable zone. When the electric pump power increases to 1300 W, the output power reaches 96 W.

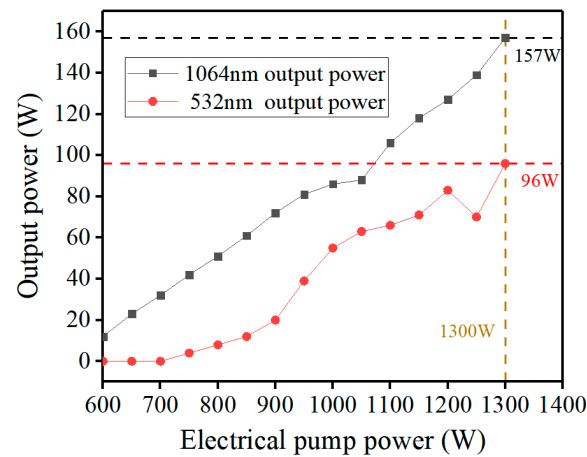


**Figure 5.** The output power of the 1064 nm laser and 532 nm laser under different pump currents.

The pulse width of the 532 nm laser was measured by a pulse detector (THORLABS, DET10A2) and digital oscilloscope (Tektronix, TDS 3054B). Figure 6a shows the pulse width of the laser at 532 nm as a function of pumping current. From Figure 6a, we can see that the pulse width of the 532 nm laser decreased with the pumping current. The pulse width of the green laser, as shown in Figure 6b, is 55.8 ns at the maximal output power and the repetition rate of 10 kHz.

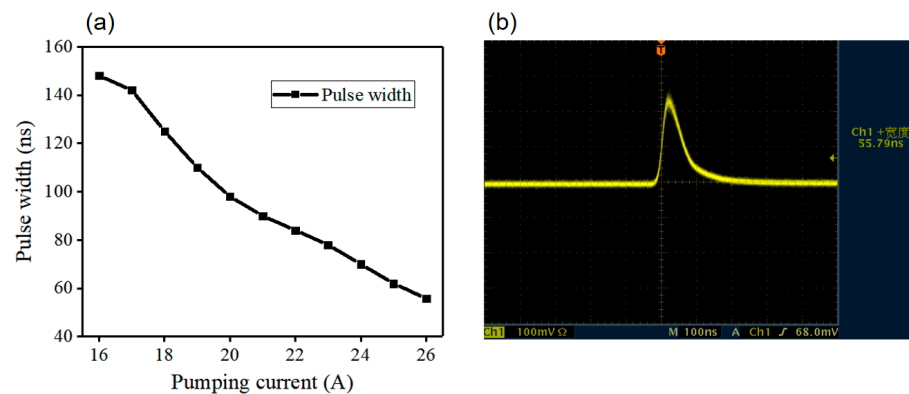


**Figure 6.** (a) Variation of the pulse width as a function of pumping current. (b) A typical recorded pulse shape at the maximum output green power.

A beam quality diagnostic instrument (DataRay, M2DU-200 Stage) was used to measure the spot and beam quality of the laser, as shown in Figure 7. Figure 7a shows the recorded spatial profile of the output green beam, which is nearly circular, when the power of the 532 nm laser is 96 W. Figure 7a also shows the relative distribution of the 532 nm laser, which is 70 cm from the output mirror when the output power is 96 W. This shows that the far-field spot of the laser output has approximately the same spatial distribution as the TEM<sub>00</sub> mode. To measure the beam quality of the laser, the output beam was exposed to the CCD camera after passing through an internal lens with a 100 mm focus length. In Figure 7b, the variation in the M<sup>2</sup> value of the green beam is shown as a function of the output green power. The M<sup>2</sup> value is shown to increase with the increase in the power of 532 nm laser. Figure 7c shows a horizontal beam quality of M<sup>2</sup><sub>x</sub> = 5.98 and vertical beam quality of M<sup>2</sup><sub>y</sub> = 8.14 when the output power of the 532 nm laser is 96 W.

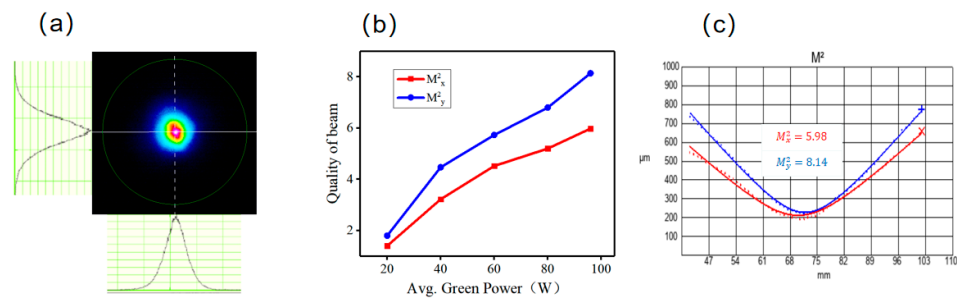


**Figure 7.** (a) Recorded spatial profile of the green beam. (b) Measured variation in the  $M^2$  value of the green beam as a function of the green output power. (c) The beam quality of 96 W.

This variation in the  $M^2$  value with the output power of 532 nm can be qualitatively explained using the estimated variation in the fundamental  $TEM_{00}$  mode radius at the Nd:YAG rod, as a function of the pump power. The  $M^2$  value varies inversely with the fundamental  $TEM_{00}$  mode area at the pumped Nd:YAG rod [22]. At a low pumping current, the  $TEM_{00}$  mode radius at the gain medium is large, which leads to a lower  $M^2$  value. As the pumping current is increased, the mode radius decreases with the pumping current due to the thermal lensing effect at the gain medium, which leads to a rapid increase in the  $M^2$  value of the green beam.

From the perspective of practical applications, brightness ( $B$ ) is also a very important factor for lasers, which is defined as [23]:

$$B = \frac{C * P}{\lambda^2 * M_x^2 * M_y^2} \quad (7)$$

where  $P$  represents the average output power and  $C$  is a constant depending on the beam profile ( $C = 1$  for a Gaussian-type beam). The brightness of the laser was calculated to be  $6.97 \times 10^8 \text{ W}\cdot\text{cm}^{-2}\cdot\text{Sr}$ , which is 1.13, 4, and 6.5 times higher than that in other works, such as in [14] (164 W,  $M_x^2 = 9.52$ ,  $M_y^2 = 9.86$ ,  $B = 6.17 \times 10^8 \text{ W}\cdot\text{cm}^{-2}\cdot\text{Sr}$ ), [15] (160 W,  $M^2 = 18$ ,  $B = 1.74 \times 10^8 \text{ W}\cdot\text{cm}^{-2}\cdot\text{Sr}$ ), and [12] (121 W,  $M^2 = 20$ ,  $B = 1.07 \times 10^8 \text{ W}\cdot\text{cm}^{-2}\cdot\text{Sr}$ ), respectively.

## 5. Conclusions

In conclusion, we developed an intracavity frequency-doubled acousto-optic Q-switch Nd:YAG laser. Our laser can produce up to 96 W of power at 532 nm at a 10 kHz repetition rate, with a 55.8 ns pulse duration. Meanwhile, the beam quality factors  $M_x^2 = 5.98$ ,  $M_y^2 = 8.14$  were measured at the maximum output power, corresponding to a brightness of  $6.97 \times 10^8 \text{ W}\cdot\text{cm}^{-2}\cdot\text{Sr}$ . To the authors' knowledge, this is the highest brightness obtained for a high-power, double-intracavity-frequency, Q-switched Nd:YAG laser. Due to its high power, good beam quality, and high brightness, the laser has good application prospects in the laser-processing field. For example, the laser can be used a hybrid laser system, using a water jet as light guide. The stable water jet thus works as a liquid waveguide delivering laser light to the work piece, avoiding thermal damage to the sample.

**Author Contributions:** Conceptualization, X.L.; Methodology, X.L.; Validation, H.L. and B.Y.; Formal analysis, B.Y.; Resources, Q.L.; Data curation, J.H.; Writing – original draft, H.L.; Writing – review & editing, H.L.; Visualization, Y.L.; Supervision, Y.D. and Z.W. All authors have read and agreed to the published version of the manuscript.

**Funding:** This research was funded by Beijing Municipal Natural Science Foundation, grant number 1212009; Basic Scientific Research, grant number JCKY2021110B175; Open Fund for Key Laboratory of Solid-State Laser Technology.

**Institutional Review Board Statement:** Not applicable.

**Informed Consent Statement:** Not applicable.

**Data Availability Statement:** Not applicable.

**Conflicts of Interest:** The authors declare no conflict of interest.

## References

1. Siva Prasad, H.; Brueckner, F.; Volpp, J.; Kaplan, A.F. Laser metal deposition of copper on diverse metals using green laser sources. *Int. J. Adv. Manuf. Technol.* **2020**, *107*, 1559–1568. [[CrossRef](#)]
2. Peng, S.Y.; Kang, H.W.; Pirzadeh, H.; Stinson, D. MoXy fiber with active cooling cap for bovine prostate vaporization with high power 200W 532 nm laser. In *Photonic Therapeutics and Diagnostics VII*; SPIE: Bellingham, WA, USA, 2011; Volume 7883, pp. 236–244.
3. Nisticò, S.P.; Cannarozzo, G.; Provenzano, E.; Tamburi, F.; Fazio, G.; Sannino, M.; Negosanti, F.; Del Duca, E.; Patruno, C.; Bennardo, L. Nanosecond Q-Switched 1064/532 nm Laser to Treat Hyperpigmentations: A Double Center Retrospective Study. *Clin. Pract.* **2021**, *11*, 708–714. [[CrossRef](#)] [[PubMed](#)]
4. Kun, L.; Su-Hui, Y.; Ying-Qi, L.; Xue-Tong, L.; Xin, W.; Jin-Ying, Z.; Zhuo, L. Underwater ranging with intensity modulated 532 nm laser source. *Acta Phys. Sin.* **2021**, *70*, 084203.
5. Wu, B.; Chen, N.; Chen, C.; Deng, D.; Xu, Z. Highly efficient ultraviolet generation at 355 nm in LiB<sub>3</sub>O<sub>5</sub>. *Opt. Lett.* **1989**, *14*, 1080–1081. [[CrossRef](#)] [[PubMed](#)]
6. Xu, Y.-T.; Xu, J.-L.; Guo, Y.-D.; Yang, F.-T.; Chen, Y.-Z.; Xu, J.; Xie, S.-Y.; Bo, Y.; Peng, Q.-J.; Cui, D.; et al. Compact high-efficiency 100-W-level diode-side-pumped Nd: YAG laser with linearly polarized TEM<sub>00</sub> mode output. *Appl. Opt.* **2010**, *49*, 4576–4580. [[CrossRef](#)] [[PubMed](#)]
7. Richardson, D.J.; Nilsson, J.; Clarkson, W.A. High power fiber lasers: Current status and future perspectives. *J. Opt. Soc. Am. B* **2010**, *27*, B63–B92. [[CrossRef](#)]
8. Grechin, S.G.; Nikolaev, P.P. Diode-side-pumped laser heads for solid-state lasers. *Quant. Electron.* **2009**, *39*, 1–17. [[CrossRef](#)]
9. Yi-Ting, X.; Jia-Lin, X.; Qian-Jin, C.; Shi-Yong, X.; Yuan-Fu, L.; Yong, B.; Qin-Jun, P.; Da-Fu, C.; Zu-Yan, X. High efficiency multi-kW diode-side-pumped Nd: YAG laser with reduced thermal effect. *Chin. Phys. Lett.* **2010**, *27*, 024201. [[CrossRef](#)]
10. Fujikawa, S.; Kojima, T.; Yasui, K. High-power and high-efficiency operation of a CW-diode-side-pumped Nd: YAG rod laser. *IEEE J. Sel. Top. Quantum Electron.* **1997**, *3*, 40–44. [[CrossRef](#)]
11. Kiriya, H.; Matsuoka, S.; Maruyama, Y.; Matoba, T.; Arisawa, T. Highly efficient second harmonic generation by using four pass quadrature frequency conversion. In *Advanced High-Power Lasers*; SPIE: Bellingham, WA, USA, 2000; Volume 3889, pp. 638–643.
12. Boulanger, B.; Fejer, M.M.; Blachman, R.; Bordui, P.F. Study of KTiOPO<sub>4</sub> gray-tracking at 1064, 532, and 355 nm. *Appl. Phys. Lett.* **1994**, *65*, 2401–2403. [[CrossRef](#)]
13. Zhenyu, Y.; Jianfeng, J.; Bo, T. 162W Laser Diode-Pumped Nd:YAG Intracavity-Doubled Laser. *Chin. J. Lasers* **2005**, *32*, 4.
14. Geng, A.; Bo, Y.; Bi, Y.; Sun, Z.; Yang, X.; Peng, Q.; Li, H.; Li, R.; Cui, D.; Xu, Z. One hundred and twenty one W green laser generation from a diode-side-pumped Nd:YAG laser by use of a dual-V-shaped configuration. *Opt. Lasers Eng.* **2006**, *44*, 589–596. [[CrossRef](#)]
15. Yong, B.; Qianjin, C.; Aicong, G.; Yang, X.; Peng, Q.; Lu, Y.; Cui, D.; Xu, Z. 218 W, M<sup>2</sup> = 20.2 green beam generation by intracavity-frequency-doubled diode-pumped Nd: YAG laser. In Proceedings of the 2007 Conference on Lasers and Electro-Optics (CLEO), Baltimore, MD, USA, 6–11 May 2007; pp. 1–2.
16. Zhongyao, F.; Chengrong, L.; Xiu, L.; Jun, W.; Jintao, B. Laser-Diode Side-Pumped two rods Quasi-Continuous-Wave Nd:YAG green laser. *ACTA OPTICA SINICA* **2008**, *28*, 4.
17. Sharma, S.K.; Singh, A.J.; Gupta, P.K.; Hedaoo, P.; Mukhopadhyay, P.K.; Ranganathan, K.; Bindra, K.S.; Oak, S.M. Thermal birefringence-compensated linear intracavity frequency doubled Nd: YAG rod laser with 73 ns pulse duration and 160 W green output power. *Pramana* **2014**, *82*, 191–195. [[CrossRef](#)]
18. Yuan, X.; Zhang, L.; Hu, Z.; Liu, Y.; Zhang, Z.; Yu, H.; Wu, P.; Wang, L.; Zhao, W.; Wang, Y.; et al. High power fiber-coupled acousto-optically Q-switched 532 nm laser with a side-pumped Nd: YAG laser module. *J. Opt. Technol.* **2017**, *84*, 373–376. [[CrossRef](#)]
19. Singh, A.; Sharma, S.K.; Mukhopadhyay, P.K.; Bindra, K.S. 260 W of average green beam generation by intracavity frequency-doubled acousto-optic Q-Switched Nd: YAG laser. *J. Opt.* **2019**, *48*, 512–519. [[CrossRef](#)]
20. Chen, Y.F.; Huang, T.M.; Kao, C.F.; Wang, C.L.; Wang, S. Optimization in scaling fiber-coupled laser-diode end-pumped lasers to higher power: Influence of thermal effect. *Quantum Electron. IEEE J.* **1997**, *33*, 1424–1429. [[CrossRef](#)]
21. Hodgson, N.; Weber, H. *Optical Resonators*; Springer: Berlin/Heidelberg, Germany, 1997.
22. Koehner, W. *Solid State Laser Engineering*, 6th ed.; Springer: New York, NY, USA, 2006.
23. Liu, X.; Jia, W.; Song, Y.; Yang, S.; Liu, S.; Liu, Y.; Yan, A.; Wang, Z. High energy, high brightness picosecond master oscillator power amplifier with output power 65.5 W. *Optics Express* **2020**, *28*, 8016–8026. [[CrossRef](#)] [[PubMed](#)]

**Disclaimer/Publisher’s Note:** The statements, opinions and data contained in all publications are solely those of the individual author(s) and contributor(s) and not of MDPI and/or the editor(s). MDPI and/or the editor(s) disclaim responsibility for any injury to people or property resulting from any ideas, methods, instructions or products referred to in the content.